Chemical Science

ROYAL SOCIETY OF CHEMISTRY

EDGE ARTICLE

View Article Online
View Journal | View Issue



Cite this: *Chem. Sci.*, 2023, **14**, 8076

All publication charges for this article have been paid for by the Royal Society of Chemistry

# Interface solvation regulation stabilizing the Zn metal anode in aqueous Zn batteries†

Kuo Wang,‡ Tong Qiu,‡ Lu Lin, Fangming Liu, Jiaqi Zhu, Xiao-Xia Liu and Xiaoqi Sun *

The Zn metal anode experiences dendritic growth and side reactions in aqueous zinc batteries. The regulation of the interface environment would provide efficient modification without largely affecting the aqueous nature of bulk electrolytes. Herein, we show that the ethylene carbonate (EC) additive is able to adsorb on the Zn surface from the $ZnSO_4$ electrolyte. Together with the higher dielectric constant of EC than water, $Zn^{2+}$ preferentially forms EC-rich solvation structures at the interface even with a low overall EC content of 4%. An inorganic–organic solid-electrolyte interface (SEI) is also generated. Thanks to the increased energy levels of the lowest unoccupied molecular orbital of EC-rich solvation structures and the stable SEI, side reactions are suppressed and the $Zn^{2+}$ transference number increases to allow uniform Zn growth. As a result, the cycle life of Zn stripping/plating in symmetric Zn cells extends from 108 h to 1800 h after the addition of 4% EC. Stable cycling for 180 h is realized with 35% depth of discharge in the 4% EC electrolyte, superior to the initial cell failure with EC-free electrolyte. The capacity retention of the Zn//$V_6O_{13}\cdot H_2O$ full cell with N/P = 1.3 also increases from 51.1% to 80.5% after 500 cycles with the help of EC.

Received 11th April 2023
Accepted 3rd July 2023

DOI: 10.1039/d3sc01831h

rsc.li/chemical-science



## Introduction

Rechargeable aqueous zinc batteries have been widely studied as an advanced energy storage system due to their low toxicity and low cost.[1–6] The zinc metal anode provides high theoretical capacity (820 mA h $g^{-1}$) and low redox potential (−0.76 V *vs.* SHE). However, it also experiences dendritic growth and side reactions in aqueous batteries, which hinder further developments.[7–20] The dendrite formation results from the inhomogeneous nucleation of Zn, followed by the preferential crystal growth on existing nuclei to minimize the surface energy. Side reactions, mainly the hydrogen evolution reaction (HER), are attributed to the thermodynamic instability of Zn metal in a mild acidic environment and competitive reduction of $Zn^{2+}$ and $H^+$ during the Zn deposition process.

It has been demonstrated that $Zn^{2+}$ solvation structures in electrolytes are essential in determining the deposition/dissolution behavior and any possible side reactions. Accordingly, a few strategies have been proposed to regulate the solvation structures. Dimethyl sulfoxide,[21] acetonitrile,[22,23] methanol[24] and a few carbonates[25–27] were introduced in electrolytes, respectively. They can replace the water in the $Zn^{2+}$ solvation shells, which helped guide uniform $Zn^{2+}$ deposition and inhibit the HER. These organic additives also generate solid-electrolyte interface (SEI) on the Zn electrode to further solve the related problems. Nevertheless, in order to change the $Zn^{2+}$ solvation structures in bulk electrolytes, additives need to be introduced stoichiometrically with respect to $Zn^{2+}$ to enter all solvation shells. The addition of excessive additives would sacrifice the low toxicity and low cost advantages of aqueous electrolytes.

Since Zn deposition/dissolution or side reactions take place at the interface between the Zn electrode and electrolyte, it is more efficient to regulate the interface environment in order to modify the electrochemical performance of the Zn electrode. If additives are able to accumulate at the inner Helmholtz layer of the Zn electrode and present a high tendency of coordination with $Zn^{2+}$, it would effectively change $Zn^{2+}$ solvation structures at the interface while bulk electrolytes remain aqueous. Polar solvents, in particular, are able to weaken the interactions between anions and cations. They would further enter $Zn^{2+}$ solvation shells provided that stable solvation structures can be formed. We herein introduce ethylene carbonate (EC), which possesses the dielectric constant (89.8$\varepsilon$) higher than that of most reported organic solvents (Fig. 1) and corresponds to larger polarity, as the additive to the typical 3 m $ZnSO_4$ electrolyte (units in mol $kg^{-1}$, around 2.2 mol $L^{-1}$). Theoretical calculations and experimental analysis confirm the effective adsorption of EC on the Zn surface, which preferentially generates $ZnEC_5H_2O^{2+}$ and $ZnEC_6^{2+}$ solvation structures at the

*Department of Chemistry, Northeastern University, Shenyang 110819, China. E-mail: sunxiaoqi@mail.neu.edu.cn*

† Electronic supplementary information (ESI) available. See DOI: https://doi.org/10.1039/d3sc01831h

‡ These authors contributed equally to this work.

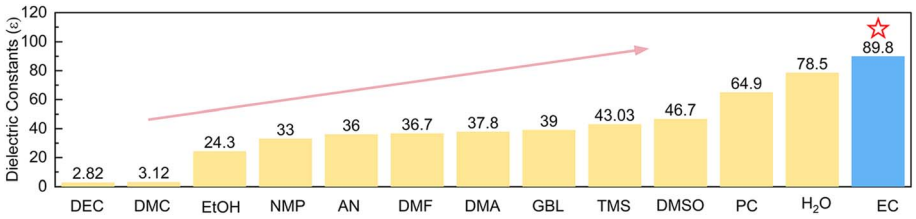


Fig. 1 Dielectric constants of EC and other common solvents including $H_2O$.

interface. They present higher energy levels of the lowest unoccupied molecular orbital (LUMO) than $Zn(H_2O)_6^{2+}$, corresponding to higher HER resistance. EC molecules also induce a stable inorganic–organic SEI layer on Zn. It further suppresses side reactions, and the $Zn^{2+}$ transference number increases to ensure uniform Zn deposition. Thanks to the above effects, the coulombic efficiencies of Zn plating/stripping reach 99.4% for 600 cycles in the 4% EC electrolyte, and the cycle life of symmetric Zn cells extends from 108 h to 1800 h at 1 mA $cm^{-2}$ and 1 mA h $cm^{-2}$ after the addition of EC. Importantly, Zn stripping/plating with 35% depth of discharge (DOD) achieves a cycle life of 180 h in 4% EC, which is superior to the initial failure of the cell with EC-free electrolyte. The capacity retentions of $Zn//V_6O_{13}\cdot H_2O$ full batteries with N/P = 1.3 (based on theoretical capacities) also increase from 51.1% to 80.5% after 500 cycles with the help of EC.

## Results and discussion

The interface environment between the Zn electrode and the electrolyte is essential in determining Zn deposition behavior and possible side reactions. The influence of EC on the interface is thus first studied. The adsorption energies of EC and $H_2O$ molecules on the Zn (100) crystal plane are calculated (Fig. 2a). EC exhibits larger adsorption energy of −0.63 eV in comparison to −0.44 eV for $H_2O$, indicating that EC molecules preferentially adsorb on the Zn surface in the mixed solution containing EC and water. Fig. 2b and c show the charge density difference and 2D contour map of electron density statistics at the interface between EC and Zn. It demonstrates the transfer of electron density from EC to the surface of Zn, confirming the effective interactions. The interface environment is further studied by calculating the electrochemical double layer capacitance (EDLC) of the Zn electrode in the 3 m $ZnSO_4$ aqueous electrolyte and after adding 4% EC (labeled as w/o EC and 4% EC, respectively) with cyclic voltammetry (CV) in the non-Faraday range (Fig. S1†). According to linear fits (Fig. 2d), the Zn electrode exhibits the EDLC of 105 μF $cm^{-2}$ in 3 m $ZnSO_4$, which decreases to 43 μF $cm^{-2}$ in 4% EC. It corresponds to the increase of Stern layer distance, resulting from the replacement of water molecules by larger sized EC in the inner Helmholtz layer of the Zn electrode.[27,28] Fig. 2e shows the contact angles of 3 m $ZnSO_4$ and 4% EC solutions on Zn foil. The angles of 3 m $ZnSO_4$ change from 109.5° to 106.7° after 120 s, while those of 4% EC reduce from 90° to 84.8°. The smaller angles of the latter are attributed to the adsorption of EC molecules on Zn. The above analysis demonstrates that the interface of the Zn electrode in the 4% EC electrolyte is EC rich locally. It would generate different solvation structures for $Zn^{2+}$ at the interface from the bulk electrolyte.

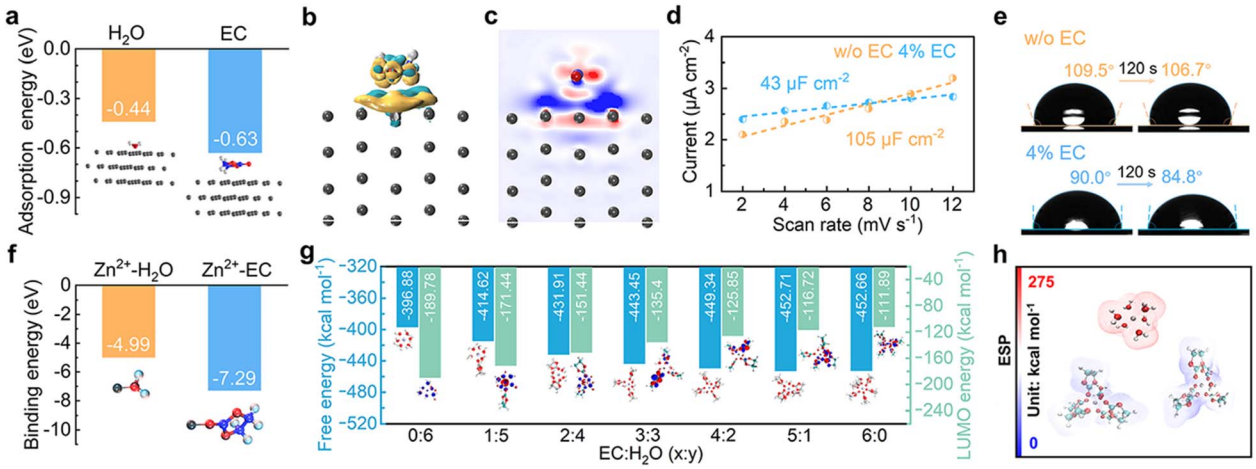


Fig. 2 (a) Adsorption energies of solvent molecules ($H_2O$ or EC) on the Zn (100) facet. (b) Charge density difference and (c) sliced 2D contour map reflecting the interactions between EC and Zn at the interface. (d) Linear fits to calculate the EDLC of Zn in different electrolytes. (e) Contact angle measurements of Zn foil in different solutions before and after 120 s. (f) Binding energies between $Zn^{2+}$ and solvent molecules ($H_2O$ or EC). (g) Free energies and LUMO energy levels of $ZnEC_x(H_2O)_y^{2+}$ ($x + y = 6$) complexes. (h) Electrostatic surface potentials of $Zn(H_2O)_6^{2+}$, $ZnEC_5H_2O^{2+}$ and $ZnEC_6^{2+}$.

The interactions between $Zn^{2+}$ and EC or $H_2O$ molecules are studied by density functional theory (DFT) calculations. It results in a much larger binding energy of $Zn^{2+}$–EC than $Zn^{2+}$–$H_2O$ (−7.29 eV *vs.* −4.99 eV, Fig. 2f), suggesting the favorable coordination of $Zn^{2+}$ with EC. The free energies of $ZnEC_x(H_2O)_y^{2+}$ ($x + y = 6$) complexes with different $x$ and $y$ values are calculated, and results are summarized in Fig. 2g. $SO_4^{2-}$ is not included for the calculation due to its low participation in the inner solvation shells of $Zn^{2+}$ as confirmed by molecular dynamics (MD) simulation and Raman analysis (Fig. S2†). With the substitution of solvated water by EC, the free energy decreases from −396.88 kcal $mol^{-1}$ for $Zn(H_2O)_6^{2+}$ to −452.71 kcal $mol^{-1}$ and −452.66 kcal $mol^{-1}$ for $ZnEC_5H_2O^{2+}$ and $ZnEC_6^{2+}$, respectively, which corresponds to increased stability. In accordance, the electrostatic surface potentials of $Zn(H_2O)_6^{2+}$, $ZnEC_5H_2O^{2+}$ and $ZnEC_6^{2+}$ show that the solvation structures are more stable with EC molecules replacing water in the coordination shell (Fig. 2h).[29] The results demonstrate that $ZnEC_5H_2O^{2+}$ and $ZnEC_6^{2+}$ are the favorable species at the EC-rich interface of the Zn electrode, despite the low overall EC concentration in the bulk electrolyte.

According to previous studies, the solvated water around $Zn^{2+}$ is mainly responsible for the HER side reaction at the Zn electrode.[30] The LUMO energy levels of $ZnEC_x(H_2O)_y^{2+}$ species are calculated. As shown in Fig. 2g, the LUMO level increases with more EC replacing water in the solvation shell, corresponding to more difficult reduction. Therefore, the formation of $ZnEC_5H_2O^{2+}$ and $ZnEC_6^{2+}$ structures instead of $Zn(H_2O)_6^{2+}$ at the interface helps to suppress HER side reactions. Meanwhile, MD simulation and spectroscopy analysis also suggest the formation of hydrogen bonds among EC and water molecules (Fig. S3†). It further helps to reduce water activity and inhibit the HER.

The EC species at the interface, both the ones solvated with $Zn^{2+}$ and free molecules, may generate SEI on the Zn electrode over electrochemical cycling. This is studied by Fourier transform infrared (FT-IR) spectroscopy with the reflection mode on a Zn electrode after 25 stripping/plating cycles (2 mA $cm^{-2}$, 2 mA h $cm^{-2}$). As shown in Fig. 3a, the stretching vibrations of C–O at 1079 $cm^{-1}$, 1107 $cm^{-1}$ and 1155 $cm^{-1}$ are attributed to ether from PEO-type polymers, alkyl carbonate salts ($(ROCO_2)_2Zn$) and alkyl carbonate (R–O–CO–O–R), respectively.[31] The bending vibration of –$CH_2$– shows up at 1457 $cm^{-1}$, and the stretching vibration of carbonate from $ZnCO_3$ shows up at 1540 $cm^{-1}$.[32] The stretching vibrations of C=O from alkyl carbonate salts and alkyl carbonate appear at 1633 $cm^{-1}$ and 1740 $cm^{-1}$, respectively.[33] The above species originate from EC decomposition on the Zn electrode.

The SEI composition is further studied by X-ray photoelectron spectroscopy (XPS) with different etching depths. In the C 1s spectrum of an un-etched electrode (Fig. 3b), signals from C–O–C, R–O–CO–O–R, $(ROCO_2)_2Zn$ and $ZnCO_3$ are noted.[34] With the increase of etching depth, $ZnCO_3$ disappears and the intensities of other components decrease in comparison to adventitious carbon. In the Zn 2p spectra (Fig. 3c), the un-etched electrode shows mainly the $Zn^{II}$ signal, which is attributed to $(ROCO_2)_2Zn$ and $ZnCO_3$. The $Zn^{II}$ signal decreases and

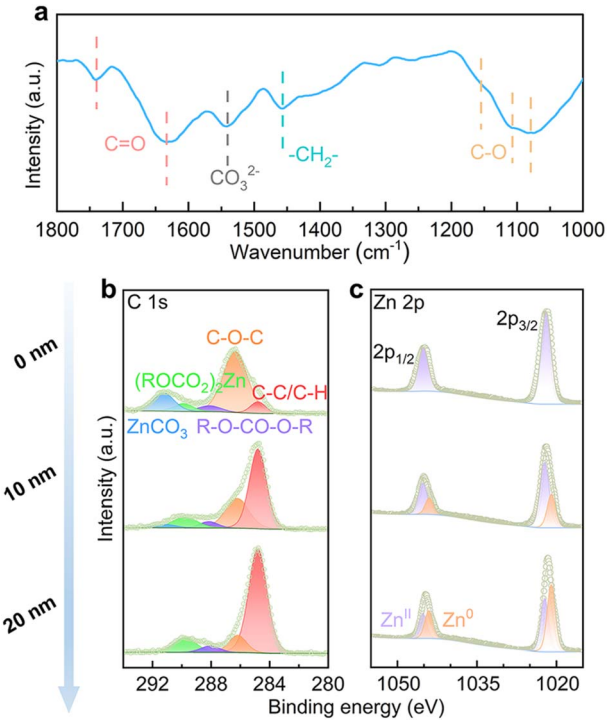


Fig. 3 (a) FT-IR, (b) C 1s and (c) Zn 2p XPS with different sputtering depths by $Ar^+$ of the Zn electrode after 25 cycles in the 4% EC electrolyte.

$Zn^0$ increases upon etching, as a result of the removal of coverage on Zn metal. Overall, the analysis suggests that the inner SEI contains PEO-type polymers, alkyl carbonate and $(ROCO_2)_2Zn$, and additional $ZnCO_3$ is found on the top surface.

The effect of EC interface regulation on the stability of the Zn electrode is studied. The HER behaviors of Zn in the two solutions are explored by *in situ* pH measurements (Fig. 4a and b). Symmetrical Zn//Zn cells are assembled, and the evolutions of electrolyte pH are monitored during the repeated galvanostatic Zn stripping/plating process. In the 3 m $ZnSO_4$ electrolyte, the pH increases from 3.79 to 3.83 during the initial rest period. It results from the chemical displacement reaction between the proton and Zn. When the current turns on, the pH values keep increasing during both stripping and plating processes. It results from the continuous chemical displacement reaction as well as the electrochemical HER process. In the 4% EC electrolyte, the initial pH is slightly higher than the neat solution. The pH change is below 0.05 after the rest period as well as stripping/plating processes. It demonstrates the effective suppression of the HER with the help of EC. Fig. 4c shows the X-ray diffraction (XRD) patterns of Zn electrodes after soaking for 24 h in the two electrolytes or after 25 galvanostatic stripping/plating cycles (2 mA $cm^{-2}$, 2 mA h $cm^{-2}$). The Zn electrodes from 3 m $ZnSO_4$ present apparent diffractions from zinc basic salts, as a result of local pH increase from chemical and electrochemical HER processes. In contrast, no such peaks are observed from the 4% EC electrolyte thanks to the inhibited HER. Fig. S4† shows the electrochemical window of the two electrolytes. The extended window on both sides of 4% EC

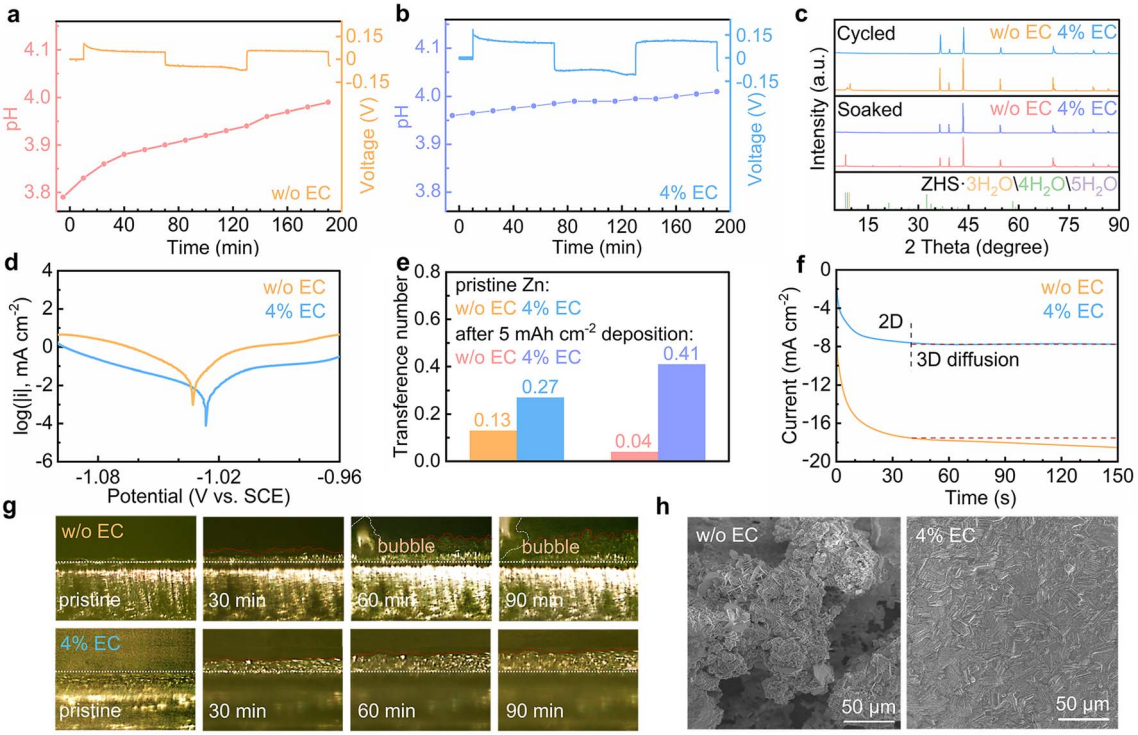


Fig. 4 *In situ* pH measurements of (a) 3 m $ZnSO_4$ and (b) 4% EC electrolytes during the Zn stripping/plating process. (c) XRD patterns of Zn soaked for 24 h and after 25 cycles, (d) Tafel plots of the Zn electrode, (e) $Zn^{2+}$ transference numbers with the pristine Zn electrode and after 5 mA h $cm^{-2}$ deposition, (f) CA curves at −150 mV *vs.* Zn constant potential, (g) *in situ* optical microscopy images during Zn deposition, and (h) SEM images of the Zn electrode after 25 cycles in $ZnSO_4$ and 4% EC electrolytes.

confirms the enhanced HER resistivity as well as suppressed oxygen evolution reaction (OER) by EC. Fig. 4d shows the Tafel plots. EC enables a decrease of corrosion current from 17.47 μA $cm^{-2}$ to 3.27 μA $cm^{-2}$ and an increase of corrosion potential from −1.033 V to −1.026 V (*vs.* SCE). This inhibited corrosion is attributed to the replacement of water by EC in the solvation shell of $Zn^{2+}$ at the interface, as well as the prevented contact between Zn and the electrolyte by the SEI.

The effect of EC on $Zn^{2+}$ transport is evaluated by calculating the transference numbers of the $Zn^{2+}$ cation (Fig. S5† and 4e).[35,36] The $Zn^{2+}$ transference numbers in $ZnSO_4$ without and with EC are 0.13 and 0.27 with the pristine Zn electrode. The higher value of the latter is attributed to the interactions between $Zn^{2+}$ and EC at the interface. Deposition processes are then carried out on the Zn electrode in the two electrolytes for 5 mA h $cm^{-2}$ capacity, which at the same time generates the stable SEI or side products on the Zn surface. The transference number in the 4% EC electrolyte increases to 0.41. It suggests that the SEI helps to further enhance $Zn^{2+}$ transport. In $ZnSO_4$, in contrast, the transference number decreases to 0.04. This hindered $Zn^{2+}$ transport is attributed to the side products of zinc basic salts formed in the EC-free electrolyte. The above experiments confirm that the SEI on Zn helps to facilitate $Zn^{2+}$ transport. It would reduce the cation gradient and regulate Zn deposition behaviors. Chronoamperometry (CA) is carried out to study the deposition process (Fig. 4f). With the constant potential of −150 mV *vs.* Zn, the deposition current density continuously increases for more than 150 s in the 3 m $ZnSO_4$ electrolyte, corresponding to the formation of uneven Zn deposits. In comparison, the current density exhibits negligible change after the initial 40 s in the 4% EC electrolyte. It results from the inhibition of lateral diffusion of Zn on the surface, which ensures uniform Zn deposition.[37,38]

*In situ* optical microscopy is applied to monitor the $Zn^{2+}$ deposition behavior. Fig. 4g shows images of the Zn interface in the two electrolytes. In 3 m $ZnSO_4$, irregular deposits appear with the increase of deposition time, and bubbles are also generated from the HER. In contrast, Zn deposited from 4% EC grows uniformly on the surface. The smaller thickness than in $ZnSO_4$ suggests denser deposition. No corrosion behavior is noted, either. Fig. 4h shows the scanning electron microscopy (SEM) images of the Zn electrode after 25 stripping/plating cycles (2 mA $cm^{-2}$, 2 mA h $cm^{-2}$). The deposits aggregate on the surface of Zn from the 3 m $ZnSO_4$ electrolyte, whereas a smooth and uniform Zn surface is obtained from 4% EC.

The electrochemical performance of Zn stripping/plating in different electrolytes is evaluated in symmetric Zn//Zn cells. The 4% EC additive is confirmed to be optimal by the cycling tests at 2 mA $cm^{-2}$ and 2 mA h $cm^{-2}$ (Fig. 5a), and further comparisons are made between EC-free and 4% EC electrolytes. Fig. 5b shows the voltage curves at current densities from 0.5 mA $cm^{-2}$ to 5 mA $cm^{-2}$ and a capacity of 2 mA h $cm^{-2}$. In the 3 m $ZnSO_4$ electrolyte, the cell short circuits at the current density of 2 mA $cm^{-2}$. In contrast, the cell with 4% EC electrolyte functions

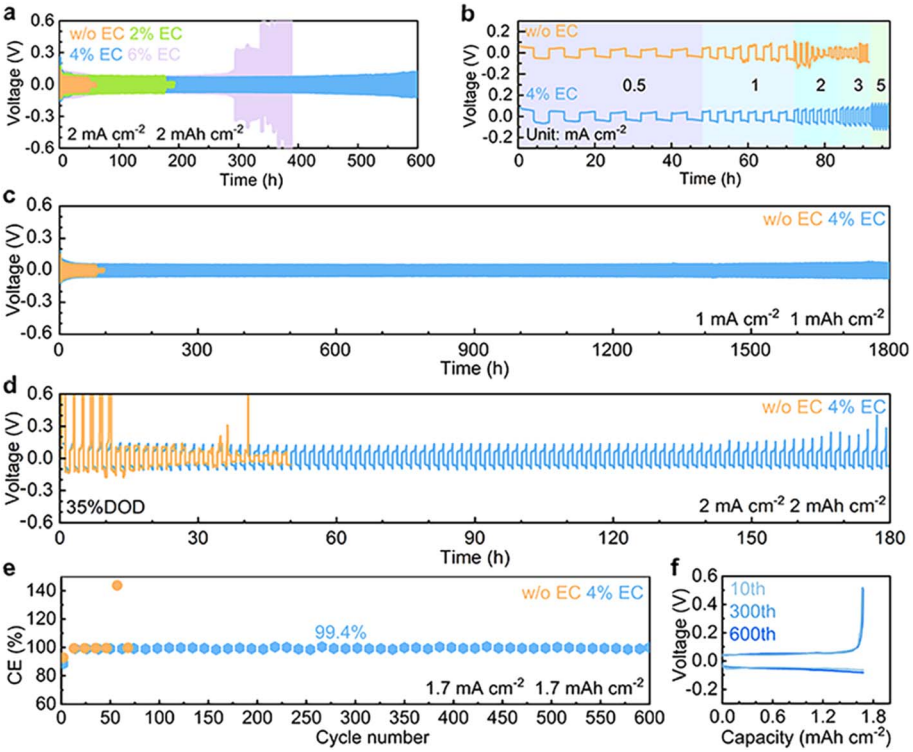


Fig. 5 (a) Long-term cycling at 2 mA $cm^{-2}$ and 2 mA h $cm^{-2}$ in 3 m $ZnSO_4$ electrolyte and with different concentrations of the EC additive. (b) Rate performance, (c) long-term cycling at 1 mA $cm^{-2}$ and (d) cycling stability with 35% DOD (thin foil) of Zn stripping/plating in Zn//Zn symmetric cells with 3 m $ZnSO_4$ and 4% EC electrolytes. (e) Coulombic efficiencies of Zn plating/stripping in Zn//Cu cells in the two electrolytes and (f) voltage curves in 4% EC.

properly at all current densities. Long-term cycling is carried out at 1 mA $cm^{-2}$ and 1 mA h $cm^{-2}$ (Fig. 5c). In $ZnSO_4$, cell short-circuiting takes place at 108 h. The cycle life extends 16.7 times to 1800 h after EC addition. This performance is competitive with previous studies (Table S1†). Symmetric cells are further assembled with thin Zn electrodes (9.7 μm), and stripping/plating is carried out at 2 mA $cm^{-2}$ current density and 2 mA h $cm^{-2}$ capacity, which corresponds to 35% DOD (Fig. 5d). In 3 m $ZnSO_4$, the voltage of the cell fluctuates greatly from the beginning. By contrast, the cell with 4% EC electrolyte exhibits 180 h stable cycles. The shorter lifetime obtained at 2 mA $cm^{-2}$ and 2 mA h $cm^{-2}$ in comparison to 1 mA $cm^{-2}$ and 1 mA h $cm^{-2}$ should be attributed to the higher depth of stripping/plating and potential sand behavior.[39] In addition to EC, other carbonate additives including propylene carbonate (PC), diethyl carbonate (DEC), ethyl methyl carbonate (EMC) and dimethyl carbonate (DMC) also extend the cycle life of symmetric cells (Fig. S6†). Nevertheless, the best performance is obtained with EC. The Zn plating/stripping coulombic efficiencies are evaluated on Cu current collectors (Fig. 5e, f and S7†). The cell with the 3 m $ZnSO_4$ electrolyte fails at the 72nd cycle, whereas the one with 4% EC delivers a stabilized CE of 99.4% for more than 600 cycles.

The 4% EC electrolyte is finally applied to a $V_6O_{13}\cdot H_2O$ cathode in zinc cells. Galvanostatic charge and discharge are carried out at different current densities (Fig. 6a and b). In the 4% EC electrolyte, the cathode delivers a high capacity of 518 mA h $g^{-1}$ at 0.1 A $g^{-1}$, and 234 mA h $g^{-1}$ capacity is retained with the increase of current density to 6 A $g^{-1}$. By contrast, the cathode with 3 m $ZnSO_4$ electrolyte exhibits much faster capacity decay at 0.1 A $g^{-1}$ as well as poorer rate performance, and only 49 mA h $g^{-1}$ capacity is left at 6 A $g^{-1}$. Fig. 6c compares the contact angles of the two electrolytes on the $V_6O_{13}\cdot H_2O$ cathode. The contact angles with $ZnSO_4$ decrease from 154.7° to 130.7° after 120 s rest. By contrast, a much smaller angle 47.6° is obtained at the initial contact between 4% EC electrolyte and $V_6O_{13}\cdot H_2O$, which further decreases to 9.5° after 120 s. This greatly improved wettability by EC helps to reduce interfacial resistance, which ensures excellent rate capability.

Long-term cycling is carried out at 5 A $g^{-1}$ (Fig. 6d and S8†). The $V_6O_{13}\cdot H_2O$ cathode realizes 86.4% capacity retention after 1500 cycles in 4% EC, which is superior to 59.7% obtained in $ZnSO_4$. The cycling stabilities are further evaluated in full cells with a limited anode of N/P = 1.3 (based on theoretical capacities). The full cell with 4% EC electrolyte exhibits 80.5% capacity retention after 500 cycles at 5 A $g^{-1}$, with an average CE of 99.9%. In comparison, only 51.1% capacity retention is obtained in the 3 m $ZnSO_4$ electrolyte (Fig. 6e and S9†). The cycling performance with the 4% EC electrolyte is also better than previously reported Zn full cells with limited anodes (Fig. 6f).[40–45] The results confirm the promoted electrochemical performance by the EC additive for not only the Zn anode but also full cells.

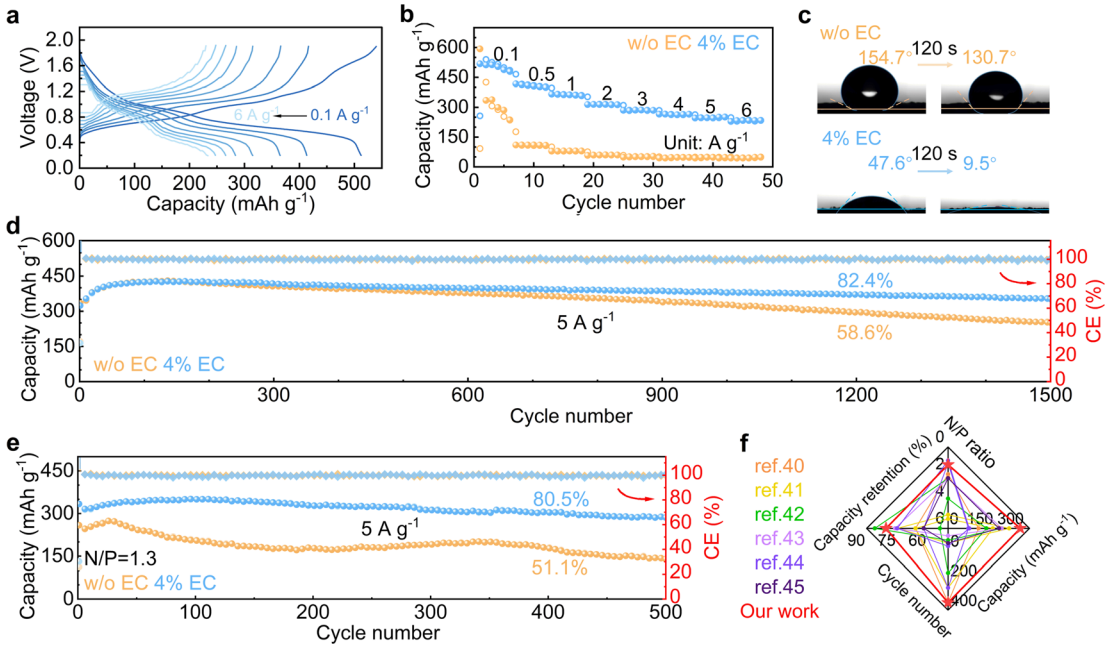


Fig. 6 (a) Charge–discharge curves of the $V_6O_{13}\cdot H_2O$ cathode in 4% EC and (b) rate performance in the two electrolytes. (c) Contact angles between the electrolytes and cathode before and after 120 s rest. Long-term cycling of $V_6O_{13}\cdot H_2O$ at 5 A $g^{-1}$ with (d) excess Zn anode and (e) limited Zn anode with N/P = 1.3. (f) Cycling performance comparison of full cells using limited Zn anodes with previous reports.

## Conclusions

In summary, we show that the regulation of $Zn^{2+}$ solvation structures at the electrode–electrolyte interface effectively enhances the electrochemical performance of the Zn anode. Specifically, the EC additive is introduced in the 3 m $ZnSO_4$ aqueous electrolyte. Theoretical calculations and experimental analysis confirm that EC preferentially adsorbs on Zn over water. EC-rich solvation structures of $Zn^{2+}$ are thus generated at the interface despite the low overall EC concentration in bulk electrolyte, and they possess higher HER resistance. An SEI layer composed of PEO-type polymers, alkyl carbonate, alkyl carbonate salts and $ZnCO_3$ is also formed on Zn from EC decomposition. The above factors not only inhibit side reactions on Zn, but also increase the $Zn^{2+}$ transference number, which ensures uniform Zn deposition. The Zn plating/stripping coulombic efficiency reaches 99.4% for more than 600 cycles in the 4% EC electrolyte. The cycle life of Zn stripping/plating in symmetric cells extends from 108 h to 1800 h at 1 mA $cm^{-2}$ and 1 mA h $cm^{-2}$ after the addition of EC. The cycle life also reaches 180 h with 35% DOD in 4% EC, whereas large voltage fluctuation is observed at the beginning in the $ZnSO_4$ electrolyte. The Zn//$V_6O_{13}\cdot H_2O$ full cell with N/P = 1.3 realizes 80.5% capacity retention after 500 cycles in 4% EC, superior to 51.1% with EC-free electrolyte. Our results show that interface regulation is an efficient way to promote the electrochemical behavior of the Zn anode. It allows the reduction of additive content so that the aqueous nature of bulk electrolyte is maintained. It would put forward new approaches for high-safety aqueous Zn batteries.

## Data availability

Data are available from the authors on reasonable request.

## Author contributions

K. W., T. Q. and X. S. conceived and designed this work. K. W. and T. Q. carried out the synthesis, electrochemical measurements and computational calculations. K. W., T. Q., L. L., F. L., J. Z. and X. L. participated in the analysis of the data. All authors discussed and revised the manuscript.

## Conflicts of interest

There are no conflicts to declare.

## Acknowledgements

This work was supported by the National Natural Science Foundation of China (52174276 and 51974070), the Liaoning Revitalization Talents Program (XLYC1907069), the Fundamental Research Funds for the Central Universities (N2105001), and the 111 Project (B16009). Special thanks are due to the instrumental analysis from the Analytical and Testing Center, Northeastern University.

## References

1 Z. Yi, G. Chen, F. Hou, L. Wang and J. Liang, Strategies for the Stabilization of Zn Metal Anodes for Zn-Ion Batteries, *Adv. Energy Mater.*, 2021, **11**, 2003065.

2 Y. Chai, X. Xie, Z. He, G. Guo, P. Wang, Z. Xing, B. Lu, S. Liang, Y. Tang and J. Zhou, A smelting–rolling strategy for ZnIn bulk phase alloy anodes, *Chem. Sci.*, 2022, **13**, 11656–11665.

3 N. Dong, F. Zhang and H. Pan, Towards the practical application of Zn metal anodes for mild aqueous rechargeable Zn batteries, *Chem. Sci.*, 2022, **13**, 8243–8252.

4 G. Ma, L. Miao, W. Yuan, K. Qiu, M. Liu, X. Nie, Y. Dong, N. Zhang and F. Cheng, Non-flammable, dilute, and hydrous organic electrolytes for reversible Zn batteries, *Chem. Sci.*, 2022, **13**, 11320–11329.

5 J. Shin, J. Lee, Y. Park and J. W. Choi, Aqueous zinc ion batteries: focus on zinc metal anodes, *Chem. Sci.*, 2020, **11**, 2028–2044.

6 L. Ma, S. Chen, N. Li, Z. Liu, Z. Tang, J. A. Zapien, S. Chen, J. Fan and C. Zhi, Hydrogen-Free and Dendrite-Free All-Solid-State Zn-Ion Batteries, *Adv. Mater.*, 2020, **32**, 1908121.

7 L. E. Blanc, D. Kundu and L. F. Nazar, Scientific Challenges for the Implementation of Zn-Ion Batteries, *Joule*, 2020, **4**, 771–799.

8 L. Geng, J. Meng, X. Wang, C. Han, K. Han, Z. Xiao, M. Huang, P. Xu, L. Zhang, L. Zhou and L. Mai, Eutectic Electrolyte with Unique Solvation Structure for High-Performance Zinc-Ion Batteries, *Angew. Chem., Int. Ed.*, 2022, **61**, e202206717.

9 Z. Hou, T. Zhang, X. Liu, Z. Xu, J. Liu, W. Zhou, Y. Qian, H. J. Fan, D. Chao and D. Zhao, A solid-to-solid metallic conversion electrochemistry toward 91% zinc utilization for sustainable aqueous batteries, *Sci. Adv.*, 2022, **8**, eabp8960.

10 J. Huang, Z. Wang, M. Hou, X. Dong, Y. Liu, Y. Wang and Y. Xia, Polyaniline-intercalated manganese dioxide nanolayers as a high-performance cathode material for an aqueous zinc-ion battery, *Nat. Commun.*, 2018, **9**, 2906.

11 J. Liu, W. Zhou, R. Zhao, Z. Yang, W. Li, D. Chao, S.-Z. Qiao and D. Zhao, Sulfur-Based Aqueous Batteries: Electrochemistry and Strategies, *J. Am. Chem. Soc.*, 2021, **143**, 15475–15489.

12 N. Liu, X. Wu, L. Fan, S. Gong, Z. Guo, A. Chen, C. Zhao, Y. Mao, N. Zhang and K. Sun, Intercalation Pseudocapacitive $Zn^{2+}$ Storage with Hydrated Vanadium Dioxide toward Ultrahigh Rate Performance, *Adv. Mater.*, 2020, **32**, 1908420.

13 A. Chen, C. Zhao, J. Gao, Z. Guo, X. Lu, J. Zhang, Z. Liu, M. Wang, N. Liu, L. Fan, Y. Zhang and N. Zhang, Multifunctional SEI-like structure coating stabilizing Zn anodes at a large current and capacity, *Energy Environ. Sci.*, 2023, **16**, 275–284.

14 Y. Shang, P. Kumar, T. Musso, U. Mittal, Q. Du, X. Liang and D. Kundu, Long-Life Zn Anode Enabled by Low Volume Concentration of a Benign Electrolyte Additive, *Adv. Funct. Mater.*, 2022, **32**, 2200606.

15 W. Sun, F. Wang, B. Zhang, M. Zhang, V. Küpers, X. Ji, C. Theile, P. Bieker, K. Xu, C. Wang and M. Winter, A rechargeable zinc-air battery based on zinc peroxide chemistry, *Science*, 2021, **371**, 46–51.

16 F. Wang, O. Borodin, T. Gao, X. Fan, W. Sun, F. Han, A. Faraone, J. A. Dura, K. Xu and C. Wang, Highly reversible zinc metal anode for aqueous batteries, *Nat. Mater.*, 2018, **17**, 543–549.

17 K. Wang, T. Qiu, L. Lin, X.-X. Liu and X. Sun, A low fraction electrolyte additive as interface stabilizer for Zn electrode in aqueous batteries, *Energy Storage Mater.*, 2023, **54**, 366–373.

18 Z. Yang, B. Wang, Y. Chen, W. Zhou, H. Li, R. Zhao, X. Li, T. Zhang, F. Bu, Z. Zhao, W. Li, D. Chao and D. Zhao, Activating sulfur oxidation reaction via six-electron redox mesocrystal $NiS_2$ for sulfur-based aqueous batteries, *Natl. Sci. Rev.*, 2022, **10**, nwac268.

19 C. Zhang, J. Holoubek, X. Wu, A. Daniyar, L. Zhu, C. Chen, D. P. Leonard, I. A. Rodríguez-Pérez, J.-X. Jiang, C. Fang and X. Ji, A $ZnCl_2$ water-in-salt electrolyte for a reversible Zn metal anode, *Chem. Commun.*, 2018, **54**, 14097–14099.

20 Y. Zhang, X. Li, L. Fan, Y. Shuai and N. Zhang, Ultrathin and super-tough membrane for anti-dendrite separator in aqueous zinc-ion batteries, *Cell Rep. Phys. Sci.*, 2022, **3**, 100824.

21 L. Cao, D. Li, E. Hu, J. Xu, T. Deng, L. Ma, Y. Wang, X. Q. Yang and C. Wang, Solvation Structure Design for Aqueous Zn Metal Batteries, *J. Am. Chem. Soc.*, 2020, **142**, 21404–21409.

22 Z. Hou, H. Tan, Y. Gao, M. Li, Z. Lu and B. Zhang, Tailoring desolvation kinetics enables stable zinc metal anodes, *J. Mater. Chem. A*, 2020, **8**, 19367–19374.

23 H. Zhao, Q. Fu, X. Luo, X. Wu, S. Indris, M. Bauer, Y. Wang, H. Ehrenberg, M. Knapp and Y. Wei, Unraveling a cathode/anode compatible electrolyte for high-performance aqueous rechargeable zinc batteries, *Energy Storage Mater.*, 2022, **50**, 464–472.

24 J. Hao, L. Yuan, C. Ye, D. Chao, K. Davey, Z. Guo and S.-Z. Qiao, Boosting Zinc Electrode Reversibility in Aqueous Electrolytes by Using Low-Cost Antisolvents, *Angew. Chem., Int. Ed.*, 2021, **60**, 7366–7375.

25 Y. Dong, L. Miao, G. Ma, S. Di, Y. Wang, L. Wang, J. Xu and N. Zhang, Non-concentrated aqueous electrolytes with organic solvent additives for stable zinc batteries, *Chem. Sci.*, 2021, **12**, 5843–5852.

26 J.-Q. Huang, X. Guo, X. Lin, Y. Zhu and B. Zhang, Hybrid Aqueous/Organic Electrolytes Enable the High-Performance Zn-Ion Batteries, *Research*, 2019, 2635310.

27 L. Miao, R. Wang, S. Di, Z. Qian, L. Zhang, W. Xin, M. Liu, Z. Zhu, S. Chu, Y. Du and N. Zhang, Aqueous Electrolytes with Hydrophobic Organic Cosolvents for Stabilizing Zinc Metal Anodes, *ACS Nano*, 2022, **16**, 9667–9678.

28 L. Zhang, L. Miao, W. Xin, H. Peng, Z. Yan and Z. Zhu, Engineering zincophilic sites on Zn surface via plant extract additives for dendrite-free Zn anode, *Energy Storage Mater.*, 2022, **44**, 408–415.

29 T. Lu and F. Chen, Multiwfn: a multifunctional wavefunction analyzer, *J. Comput. Chem.*, 2012, **33**, 580–592.

30 Q. Zhang, Y. Ma, Y. Lu, Y. Ni, L. Lin, Z. Hao, Z. Yan, Q. Zhao and J. Chen, Halogenated Zn2+ Solvation Structure for Reversible Zn Metal Batteries, *J. Am. Chem. Soc.*, 2022, **144**, 18435–18443.

31 D. Aurbach, M. L. Daroux, P. W. Faguy and E. Yeager, Identification of Surface Films Formed on Lithium in Propylene Carbonate Solutions, *J. Electrochem. Soc.*, 1987, **134**, 1611.

32 C. Pan, C. Wang, X. Zhao, P. Xu, F. Mao, J. Yang, Y. Zhu, R. Yu, S. Xiao, Y. Fang, H. Deng, Z. Luo, J. Wu, J. Li, S. Liu, S. Xiao, L. Zhang and Y. Guo, Neighboring sp-Hybridized Carbon Participated Molecular Oxygen Activation on the Interface of Sub-nanocluster CuO/Graphdiyne, *J. Am. Chem. Soc.*, 2022, **144**, 4942–4951.

33 M. K. Rahman and Y. Saito, Investigation of positive electrodes after cycle testing of high-power Li-ion battery cells: III: an approach to the power fade mechanism using FT-IR-ATR, *J. Power Sources*, 2007, **174**, 889–894.

34 K. Son, S. M. Hwang, S.-G. Woo, M. Paik, E. H. Song and Y.-J. Kim, Thermal and chemical characterization of the solid-electrolyte interphase in Li-ion batteries using a novel separator sampling method, *J. Power Sources*, 2019, **440**, 227083.

35 H. Yan, S. Li, Y. Nan, S. Yang and B. Li, Ultrafast Zinc–Ion–Conductor Interface toward High-Rate and Stable Zinc Metal Batteries, *Adv. Energy Mater.*, 2021, **11**, 2100186.

36 J.-Q. Huang, X. Lin, H. Tan, X. Du and B. Zhang, Realizing high-performance Zn-ion batteries by a reduced graphene oxide block layer at room and low temperatures, *J. Energy Chem.*, 2020, **43**, 1–7.

37 A. Bayaguud, X. Luo, Y. Fu and C. Zhu, Cationic Surfactant-Type Electrolyte Additive Enables Three-Dimensional Dendrite-Free Zinc Anode for Stable Zinc-Ion Batteries, *ACS Energy Lett.*, 2020, **5**, 3012–3020.

38 P. He and J. Huang, Chemical Passivation Stabilizes Zn Anode, *Adv. Mater.*, 2022, **34**, 2109872.

39 Z. Hou, Y. Gao, R. Zhou and B. Zhang, Unraveling the Rate-Dependent Stability of Metal Anodes and Its Implication in Designing Cycling Protocol, *Adv. Funct. Mater.*, 2022, **32**, 2107584.

40 C. Huang, X. Zhao, Y. Hao, Y. Yang, Y. Qian, G. Chang, Y. Zhang, Q. Tang, A. Hu and X. Chen, Long Shelf-Life Efficient Electrolytes Based on Trace l-Cysteine Additives toward Stable Zinc Metal Anodes, *Small*, 2022, **18**, 2203674.

41 Q. Li, Y. Wang, F. Mo, D. Wang, G. Liang, Y. Zhao, Q. Yang, Z. Huang and C. Zhi, Calendar Life of Zn Batteries Based on Zn Anode with Zn Powder/Current Collector Structure, *Adv. Energy Mater.*, 2021, **11**, 2003931.

42 D. Wang, D. Lv, H. Liu, S. Zhang, C. Wang, C. Wang, J. Yang and Y. Qian, In Situ Formation of Nitrogen-Rich Solid Electrolyte Interphase and Simultaneous Regulating Solvation Structures for Advanced Zn Metal Batteries, *Angew. Chem., Int. Ed.*, 2022, **61**, e202212839.

43 D. Wang, D. Lv, H. Peng, N. Wang, H. Liu, J. Yang and Y. Qian, Site-Selective Adsorption on $ZnF_2$/Ag Coated Zn for Advanced Aqueous Zinc–Metal Batteries at Low Temperature, *Nano Lett.*, 2022, **22**, 1750–1758.

44 J. Zheng, Q. Zhao, T. Tang, J. Yin, C. D. Quilty, G. D. Renderos, X. Liu, Y. Deng, L. Wang, D. C. Bock, C. Jaye, D. Zhang, E. S. Takeuchi, K. J. Takeuchi, A. C. Marschilok and L. A. Archer, Reversible epitaxial electrodeposition of metals in battery anodes, *Science*, 2019, **366**, 645–648.

45 J. Zhou, L. Zhang, M. Peng, X. Zhou, Y. Cao, J. Liu, X. Shen, C. Yan and T. Qian, Diminishing Interfacial Turbulence by Colloid-Polymer Electrolyte to Stabilize Zinc Ion Flux for Deep-Cycling Zn Metal Batteries, *Adv. Mater.*, 2022, **34**, 2200131.